Photoluminescence Tuning in Stretchable PDMS Film Grafted Doped Core/Multishell Quantum Dots for Anticounterfeiting

Fei Li, Xiandi Wang, Zhiguo Xia, Caofeng Pan,* and Quanlin Liu*

The development of new luminescent materials for anticounterfeiting is of great importance, owing to their unique physical, chemical, and optical properties. The authors report the use of color-tunable colloidal CdS/ZnS/ZnS:Mn^{2+}/ZnS core/multishell quantum dots (QDs)-functionalized luminescent polydimethylsiloxane film (LPF) for anticounterfeiting applications. Both luminescent QDs and as-fabricated, stretchable, and transparent LPF show blue and orange emission simultaneously, which are ascribed to CdS band-edge emission and the $^4T_1 \rightarrow {}^6A_1$ transition of Mn^{2+}, respectively; their emission intensity ratios are dependent on the power-density of a single-wavelength excitation source. Additionally, photoluminescence tuning of CdS/ZnS/ZnS:Mn^{2+}/ZnS QDs in hexane or embedded in LPF can also be realized under fixed excitation power due to a resonance energy transfer effect. Tunable photoluminescence of these flexible LPF grafted doped core/shell QDs can be finely controlled and easily realized, depending on outer excitation power and intrinsic QD concentration, which is intriguing and inspires the fabrication of many novel applications.

1. Introduction

Semiconductor quantum dots (QDs) hold excellent prospects in optoelectronics due to their transparency,[1] solution processability,[2] high efficiency,[3] and tunable band gaps.[4] These properties make them competitive building blocks for existing and emerging technologies alike. Over the past few decades, binary II–VI compound (e.g., CdS),[5] binary III–V compound (e.g., InP),[6] and ternary I–III–VI compound (e.g., $CuInS_2$)[7] QDs have been widely studied and actively applied to light-emitting diodes, lasers, solar cells, and biomarkers. In recent years, in order to avoid the toxicity of Cd^{2+} and reduce the cost of In^{3+}, perovskite QDs have become a hot topic.[8] The spectral characteristics of these QDs are narrow-band emission and broad absorption.[9] Meanwhile, there is an overlap between emission and absorption spectra of QDs owing to small Stokes shifts. Therefore, the spectral properties of QDs could be influenced by reabsorption, which comes from a resonance energy transfer (RET) effect.[10,11] Another strategy for modifying inherent properties of semiconductor QDs is to introduce dopants. Through doping optical activators, such as Mn^{2+} or rare earth ions, the electronic and photophysical properties of QDs could be modified. The dopant creates electronic states in the mid-gap region of the QDs and, thus, it alters charge separation and recombination dynamics. For Mn^{2+}-doped QDs, the dopant emission is restricted within the orange spectral window originating from the intrinsic $^4T_1 \rightarrow {}^6A_1$ transition of Mn^{2+}, which shows no relationship with the energy level of the host.[12] Additionally, the Mn^{2+}-doped QDs present large Stokes shifts, thus avoiding reabsorption. Therefore, the combination of semiconductor QDs and doped QDs with appropriate structure may receive interesting optical properties. In a previous study, Mn^{2+} doped in CdS/ZnS QDs with different radial positions, such as Mn^{2+} doped in the core, interface of core and shell, and shell, were investigated.[13] These Mn^{2+}-doped CdS/ZnS QDs show doped-position-related optical properties. The quantum yield (QY) of CdS-band emission is almost constant for these QDs, but the QY of Mn^{2+} emission increased with the Mn^{2+} doped away from the CdS core, which indicates the effective energy interaction between band-edge emission and Mn^{2+}-ion emission.

Therefore, there is a possible strategy to tune the photoluminescence (PL) of core/multishell QDs containing both band-edge emission and electronic transition from the activators, which show different luminescence behaviors depending on the excitation power. Such a luminescence material can demonstrate potential application for anticounterfeiting labels; however, it is intrinsically different from an anticounterfeiting feature relying on photoluminescence from the rare-earth-doped luminescence materials.[14] Moreover, the integration of luminescence materials on stretchable substrates currently becomes an extensively investigated topic because they offer

Dr. F. Li, Prof. Z. Xia, Prof. Q. Liu
The Beijing Municipal Key Laboratory of New Energy Materials and Technologies
School of Materials Sciences and Engineering
University of Science and Technology Beijing
Beijing 100083, P. R. China
E-mail: xiazg@ustb.edu.cn
Dr. X. Wang, Prof. C. Pan
Beijing Institute of Nanoenergy and Nanosystems
Chinese Academy of Sciences
CAS Center for Excellence in Nanoscience
National Center for Nanoscience and Technology (NCNST)
Beijing 100083, P. R. China
E-mail: cfpan@binn.cas.cn

DOI: 10.1002/adfm.201700051

the characteristics of luminescence properties and the ability to be stretched into arbitrary shapes.[15,16] Nowadays, the most studied stretchable devices are applied in artificial intelligence,[17] artificial human skin,[18] semiconductor device,[16,19] and sensor.[20] However, there are a few reports focusing on a stretchable anticounterfeiting device which can be integrated into polymer high-value documents, providing an advanced anticounterfeiting feature.

In this study, we present a stretchable and transparent excitation-power dependent, color-tunable luminescent polydimethylsiloxane (PDMS) film (LPF), and explore its potential application for anticounterfeiting. Such an LPF was fabricated by combination of a PDMS substrate and excitation-power-dependent, color-tunable QDs. The QDs, CdS/ZnS/ZnS:Mn^{2+}/ZnS, show blue and orange emission simultaneously, which are ascribed to the CdS band-edge emission[21] and $^4T_1 \rightarrow {}^6A_1$ emission of the Mn^{2+} ion,[22] respectively, and their emission intensity ratios are dependent on the power of a single-wavelength excitation source. Such a unique feature is very difficult to replicate and holds promise in the field of advanced anticounterfeiting, compared with the traditional rare earth luminescent materials with unicolor photoluminescence behavior upon external excitation.[14] Furthermore, the photoluminescence tuning of QDs can also be realized through varying QD concentration in the substrate under fixed excitation power, due to the different RET responsiveness of CdS and Mn^{2+} emission. A bottom-up method is employed to fabricate LPF, which enables facile transfer ability to any other carrier. Meanwhile, the performance of a stretchable and transparent LPF leads to its wide usage in real life anticounterfeiting. LPF can incorporate with the carrier perfectly and has no effect on the recognition of its original information, which reveals a new level of fluorescent anticounterfeiting features.

2. Results and Discussion

Synthesis illustration and structural characterizations of CdS/ZnS/ZnS:Mn^{2+}/ZnS core/multishell QDs are shown in **Figure 1**. The QDs were prepared using a three-step synthesis process, and the synthetic method is schematically shown in Figure 1a. Firstly, the CdS core was prepared when precursors of S powder and cadmium myristate, as well as solvent 1-octadecene (ODE), were loaded in a three-necked flask and heated to 250 °C under N_2 flow. Within 20 mins, the CdS band-edge emission evolves at 440 nm. However, a lower intensity broad emission centered at ≈570 nm also appeared (Figure S1i, Supporting Information), presumably due to surface trap emissions. Secondly, the CdS/ZnS core/shell QDs were synthesized by overcoating a layer of ZnS shell on a CdS core. The above CdS core was redispersed in a mixed solvent of oil amine (OLA) and ODE in a three-necked flask, which was filled with N_2, and the mixture was heated to 220 °C. Then, the zinc precursor and S precursor were injected into the solution in two batches, followed by annealing at 220 °C for 10 mins after each batch. Further injection of zinc precursor and S precursor removes the broad emission and enhances the CdS band-edge emission, as shown in Figure S1ii in the Supporting Information, which

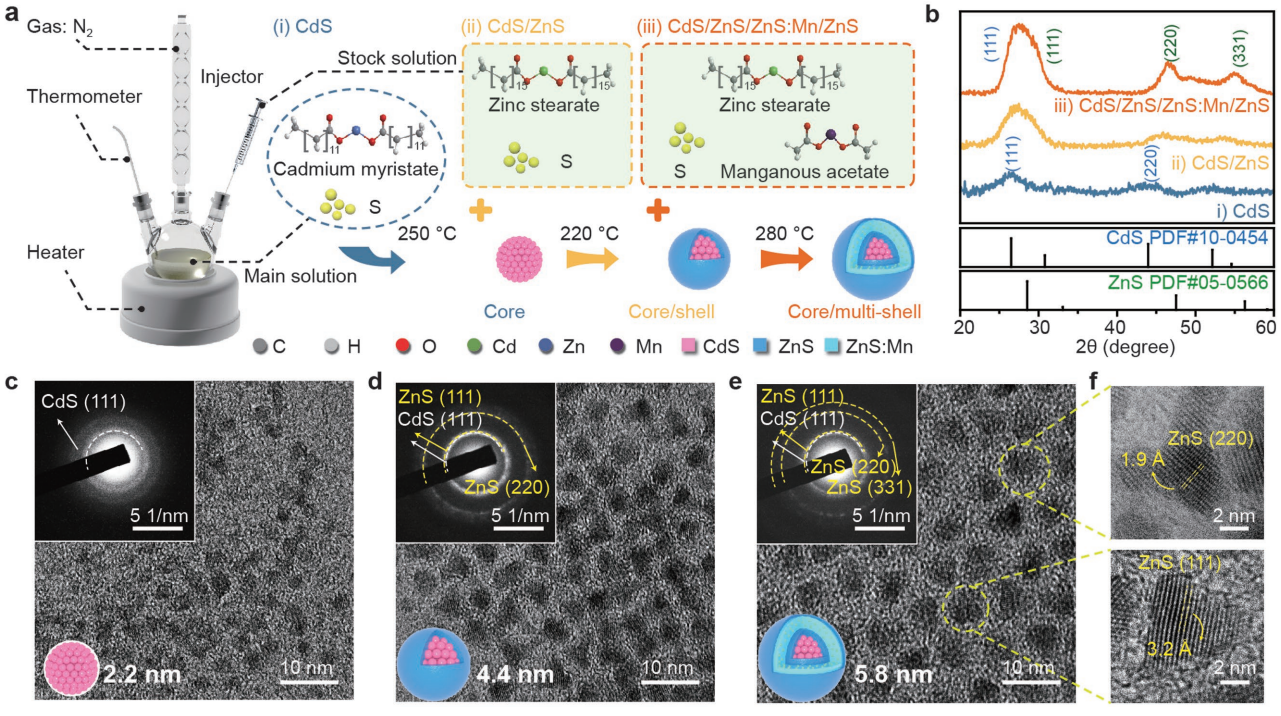

Figure 1. Synthesis illustration and structural characterizations of CdS/ZnS/ZnS:Mn^{2+}/ZnS core/multishell QDs. a) Illumination of the three-step process was demonstrated, and the hot-injection reaction and the raw materials used in each step were given; b) XRD patterns of as-prepared CdS, CdS/ZnS, and CdS/ZnS/ZnS:Mn^{2+}/ZnS QDs obtained in each step and the corresponding standard patterns of ZnS and CdS; TEM images and their electron diffraction patterns of c) CdS, d) CdS/ZnS, and e) CdS/ZnS/ZnS:Mn^{2+}/ZnS QDs; f) HRTEM images of (220) and (111) crystal face of ZnS in CdS/ZnS/ZnS:Mn^{2+}/ZnS QDs.

demonstrates the formation of a CdS/ZnS core/shell structure. The synthesis process of CdS/ZnS/ZnS:Mn^{2+}/ZnS core/multishell QDs was similar to that of CdS/ZnS QDs, and the specific synthesis process described in the experimental section. The orange emission appears after the overcoating of ZnS:Mn^{2+} on the CdS/ZnS core/shell QDs (Figure S1iii, Supporting Information). There is also a ZnS shell that is coated on the outmost layer to guarantee the highly efficient emission of ZnS:Mn^{2+}. Moreover, a tiny blue-shifting of the CdS band-edge emission toward shorter wavelength after the overcoating reaction indicates the continuous growth of a multishell. To identify the core/multishell structure, we firstly investigated the crystallographic property by powder X-ray diffraction (XRD). Three distinct diffraction peaks can be observed from the XRD pattern of the CdS core and they matched well with those of the bulk CdS cubic structure (Figure 1b). The peaks shifted to larger angles toward the diffraction peaks of a bulk ZnS cubic structure after over coating the ZnS shell on the CdS core. Additionally, the peak of the (111) crystal face of CdS became broader and asymmetric with the growth of ZnS shell. Broadening of this diffraction peak was consistent with overlying of diffraction peaks of CdS and ZnS. The fitting of this diffraction peak was carried out and the (111) crystal face of CdS and ZnS can be distinguished, respectively (Figure S2, Supporting Information). Therefore, the core/multishell structured CdS/ZnS/ZnS:Mn^{2+}/ZnS QDs was confirmed by the results of XRD analysis.

In order to further demonstrate the structure evolution of CdS/ZnS/ZnS:Mn^{2+}/ZnS QDs, the transmission electron microscopy (TEM) and high resolution TEM (HRTEM) images of CdS core, CdS/ZnS, and CdS/ZnS/ZnS:Mn^{2+}/ZnS QDs were carried out, respectively, and shown in Figure 1c–f. The size of the as-prepared CdS core, CdS/ZnS, and CdS/ZnS/ZnS:Mn^{2+}/ZnS QDs were measured as about 2.2, 4.4, and 5.8 nm from TEM images, respectively. The combination of the results of TEM and XRD demonstrate shell growth. The size dependence of the band gap energy, $E(R)$, can be given by the following effective-mass approximation when the quantum confinement becomes effective:[23]

$$E(R) = E_g + \frac{h^2\pi^2}{2R^2}\left[\frac{1}{m_e} + \frac{1}{m_h}\right] - \frac{1.786e^2}{\varepsilon R} - 0.248E^*_{Ry} \quad (1)$$

where E_g is the bulk band gap, R is the radius of the QD, and m_e and m_h are the effective masses of electrons and holes, respectively, h is the reduced Planck constant, e is the elementary charge, ε is the bulk dielectric constant, and E^*_{Ry} is the effective Rydberg energy, which is equal to $e^4/(2\varepsilon^2h^2(m_e^{-1} + m_h^{-1}))$. Adopting $m_e = 0.2\ m_0$ (m_0 is the free electron rest mass), $m_h = 0.8\ m_0$, $\varepsilon = 5.4$, and$i = 2.42$ V, a CdS QDs with an emission peak at 440 nm has an estimated radius of 2.2 nm. The experimental peak position of CdS band-edge emission is similar to the calculated result. The selected area electron diffraction in Figure 1c–e (up left) illustrate that the as-prepared QDs have cubic zinc blended structure. The diffraction ring of the (111) crystal face becomes broadened and can be identified as two distinct crystal faces of CdS and ZnS, with an increasing ZnS shell. This can also be seen in Figure 1f, where the interplanar crystal spacing is identified as 1.9 and 3.2 Å, respectively, which corresponds to that of ZnS. The result implies that the as-designed core/multishell structure has been obtained, rather than the crystallization of a CdS core.

Photoluminescence properties and the proposed luminescence mechanisms of CdS/ZnS/ZnS:Mn^{2+}/ZnS core/multishell QDs were shown in **Figure 2**. The CdS/ZnS/ZnS:Mn^{2+}/ZnS QDs with a concentration of 0.00125 mg mL^{-1} in hexane were used to explore its photoluminescence tuning properties. As depicted in Figure 2a, the core/multishell QDs show two emission bands at about 440 nm (CdS band-edge emission) and about 590 nm (Mn^{2+} emission) under different excitation-power density irradiated by a laser. The intensity of band-edge emission of CdS (I_B) monotonically increases with the increase of excitation power. However, the intensity of the Mn^{2+}-ion emission (I_O) reaches a maximum at the excitation power of 1.32 mJ cm^{-2}. The enlarged picture in Figure 2a shows the intensity saturation part of Mn^{2+}-ion emission. The intensity of Mn^{2+}-ion emission has a slightly decrease that is attributed to instrumental error when the excitation power is beyond 10.7 mJ cm^{-2} and reaches a stable level at 80.3 mJ cm^{-2}. The variation of the intensity data originated from blue and orange emission are shown in Figure 2b. I_O is stronger than I_B when the excitation power is less than 1.32 mJ cm^{-2}, so the as-observed color is orange. With the increase of excitation power, I_B becomes stronger than I_O, which leads to photoluminescence tuning, from orange to blue. The luminous intensity is given by[24]

$$I_F = kI_0(1 - 10^{-\varepsilon lc}) \quad (2)$$

where I_F is the fluorescence intensity, I_0 is the absorbed intensity, k is the quantum yield, ε is the molar absorptivity, l is the path length, and c is the concentration of analyte. On the basis of this equation, the photoluminescence intensity should be enhanced with an increase of excitation power, without saturation, which corresponds to the CdS emission in the CdS/ZnS/ZnS:Mn^{2+}/ZnS QDs. However, I_O reaches a maximum at an excitation power of 1.32 mJ cm^{-2}. The explanation of this phenomenon is given below. As shown in Figure 2c, an increase of I_O is attributed to an increased number of Mn^{2+} at $^4T_1$. The total excitation of all Mn^{2+} dopants in the QDs results in a maximum of I_O, and the I_O remains nearly constant with a further increase of excitation power. This saturation of I_O further indicates that all the Mn^{2+} ions inside individual QDs are pumped to their excited state ($^4T_1$), and no more Mn^{2+} ions can accept energy from the excitations of QDs.[25] However, a further increase of I_B is allowed under excitation at a higher intensity. An inset of Commission Internationale de l'Eclairage (CIE) chromaticity diagram in Figure 2b shows the color coordinates of QDs under various excitation power. The CIE chromaticity coordinate gradually vary, from a yellow-green region (0.197, 0.395) to an orange area (0.242, 0.547), corresponding to the excitation power at 0.001 and 0.08 mJ cm^{-2}. Nevertheless, with the continuous increase of excitation power, the CIE chromaticity coordinate gradually varies from an orange area to a blue region, rather than to red region. This phenomenon results because the quantum efficiency of Mn^{2+} ion emission (27%) is higher than that of CdS band-edge emission (17%). The higher quantum efficiency leads to a faster growth rate of emission intensity. Therefore, the intensity of orange emission

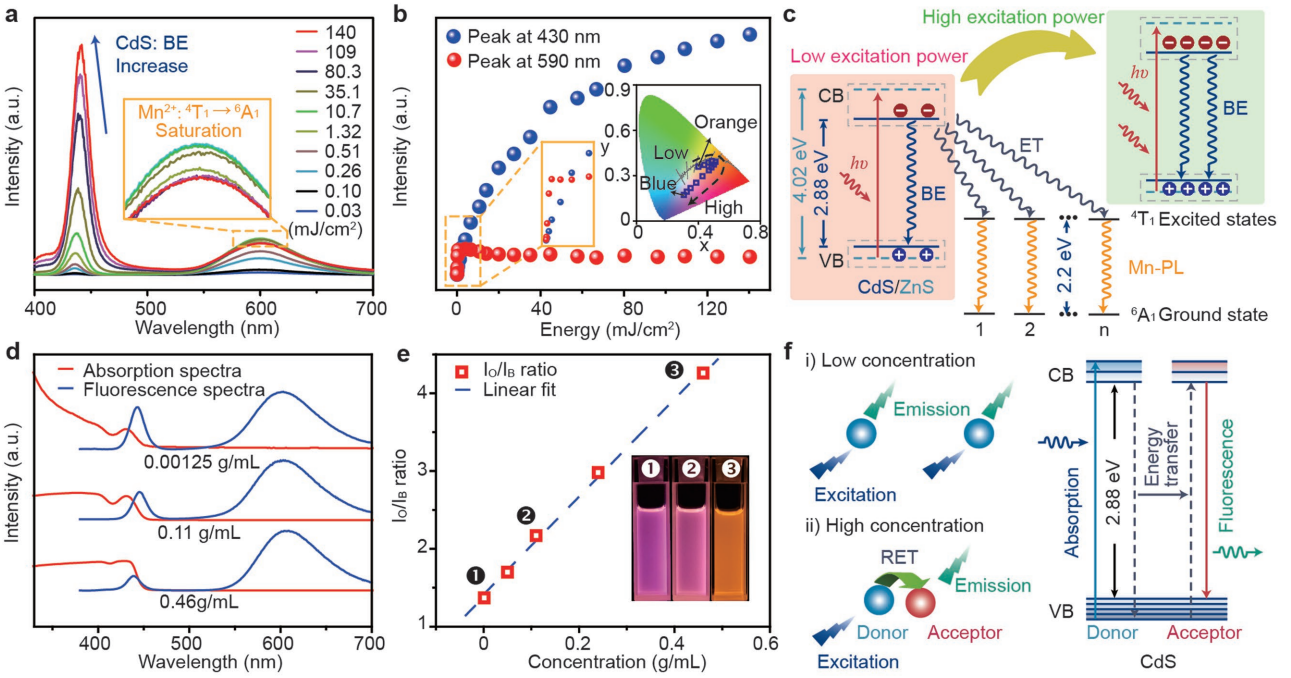

Figure 2. Photoluminescence properties and the proposed mechanisms of color-tunable CdS/ZnS/ZnS:Mn^{2+}/ZnS core/multishell QDs. a) Photoluminescence spectra and b) the emission intensity variation of CdS/ZnS/ZnS:Mn^{2+}/ZnS QDs under different excitation power (inset in (a) shows the enlarged emission peaks at near 590 nm, and inset in (b) gives the CIE 1931 chromaticity diagram and the color coordinates). c) The proposed mechanism on the excitation-power dependent variation of intensity ratio between blue and orange emission of CdS/ZnS/ZnS:Mn^{2+}/ZnS QDs. d) UV–vis absorption (red line) and photoluminescence (blue line) spectra; e) Concentration dependent orange/blue emission intensity ratios of CdS/ZnS/ZnS:Mn^{2+}/ZnS QDs in hexane (Inset: the photographs under 365 nm light irradiation of CdS/ZnS/ZnS:Mn^{2+}/ZnS QDs with a concentration of 0.0015 mg mL^{-1} (1), 0.01 mg mL^{-1} (2), and 0.5 mg mL^{-1} (3)); f) Schematic illustration of RET mechanism of CdS/ZnS/ZnS:Mn^{2+}/ZnS.

is stronger than that of blue emission before the intensity saturation of orange emission.

Photoluminescence tuning of CdS/ZnS/ZnS:Mn^{2+}/ZnS QDs can be also realized under fixed excitation power, but have variable concentration in solution due to the RET effect. Figure 2d shows the photoluminescence spectra and adsorption spectra of CdS/ZnS/ZnS:Mn^{2+}/ZnS QDs with different QD concentration in the hexane. With an increase of QD concentration, the intensity of blue emission decreases and the ratio of I_O/I_B monotonically increased, which resulted in a color change, as presented in **Figure 3**e. The inset of Figure 3e shows a photograph of the QDs with various concentrations under radiation of an *n*-UV lamp with a wavelength of 365 nm. By adjusting the concentration, these samples present different colors, suggesting that the photoluminescence emissions could be profoundly tailored. The mechanism of this phenomenon is attributed to the RET effect,[10,26] ascribed to the broad overlap of the emission and absorption spectra of CdS QDs (see in Figure 2d). A donor QD, initially in its electronic excited state, transfers energy to another acceptor QD through nonradiative dipole–dipole coupling, as shown in Figure 2f. At low concentration, the distance between QDs is much longer than the Förster distances (donor–acceptor distance of 50% RET efficiency). There are fewer opportunities for nonradiative energy transfer efficiency to take place. On the contrary, the distance between QDs was significantly shortened and enhanced the nonradiative energy transfer efficiency at high concentration. Therefore, the photoluminescence tuning can be realized by changing of the concentration of CdS/ZnS/ZnS:Mn^{2+}/ZnS QDs in the substrate. In order to understand the stability of materials as well as long lived photoluminescence behavior, we have comparatively investigated the photoluminescence emission spectra of the as-prepared CdS/ZnS/ZnS:Mn^{2+}/ZnS QDs, QDs exposed to air for 60 d, and QDs irradiated by UV light for 12 h, respectively. As given in Figure S3 in the Supporting Information, there is clearly no obvious difference in the emission intensities among them, which demonstrates good stability of as-prepared QDs for practical application.

The stretchable and transparent excitation-power-dependent, color-tunable films are fabricated by the combination of PDMS and CdS/ZnS/ZnS:Mn^{2+}/ZnS QDs via a simple solution-based technique, and, herein, PDMS can be regarded as a substrate to functionalize as-prepared QDs. Excitation-power-dependent photoluminescence spectra and variation of the blue/orange emission intensities of the LPF are shown in Figure 3. Three LPFs with different concentrations of CdS/ZnS/ZnS:Mn^{2+}/ZnS QDs are studied; the intensity of the CdS band-edge emission of the films monotonically increases with the increase of excitation power, and the intensity of Mn^{2+} emission reaches a maximum at a certain excitation power. Additionally, the inset of Figure 3a–c shows the photographs of LPF under daylight (left) and 365 nm UV light (right). The films are transparent under daylight and show different color under 365 nm UV light irradiation. The photoluminescence tuning properties of the LPFs are similar to that of QDs in hexane solution, implying the substrates have no obvious effect on the photoluminescence

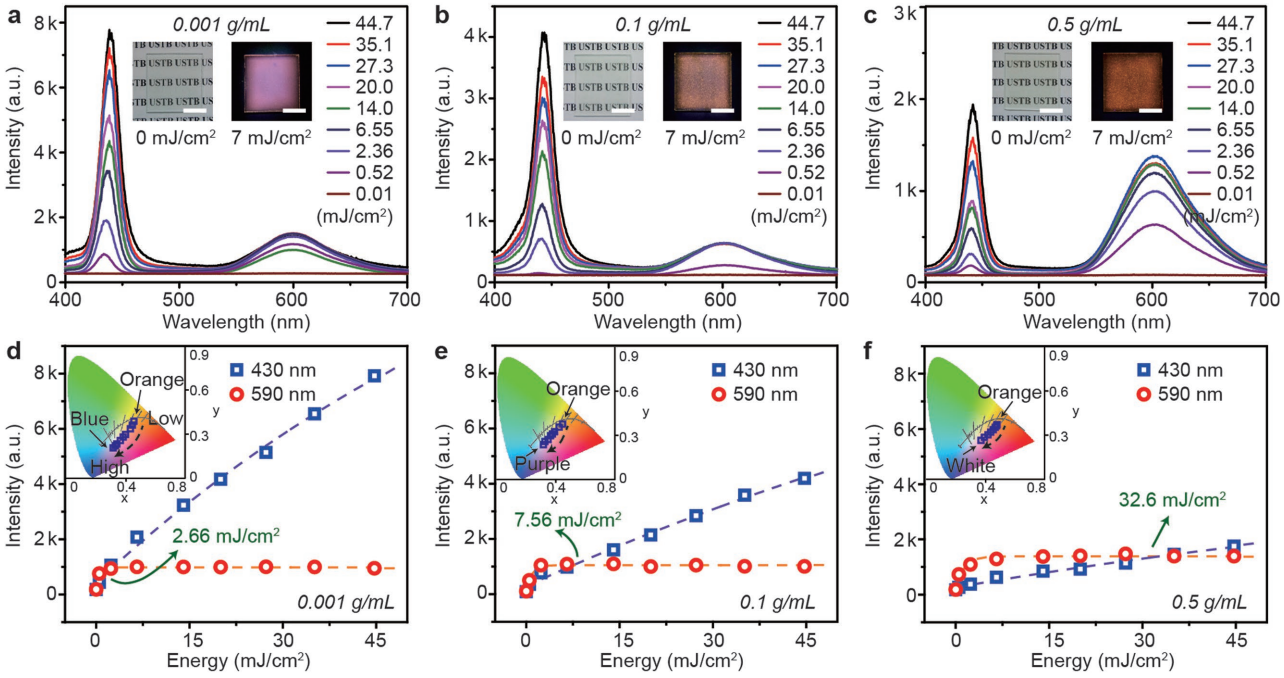

Figure 3. Excitation-power dependent photoluminescence spectra and variation of the blue/orange emission intensities of luminescent PDMS film grafted CdS/ZnS/ZnS:Mn^{2+}/ZnS QDs. Excitation-power dependent photoluminescence spectra of PDMS films with different concentrations of CdS/ZnS/ZnS:Mn^{2+}/ZnS QDs, a) 0.001 g mL^{-1}, b) 0.1 g mL^{-1}, and c) 0.5 g mL^{-1}, (inset: photographs of luminescent PDMS films under daylight (left) and 365 nm UV light (right)), scale bar: 1 cm. Variations of the blue and orange emission intensities of PDMS films depending on different excitation power. PDMS film reached the equal emission intensity of blue and orange light at different excitation powers: 2.66 mJ cm^{-2} at 0.001 g mL^{-1}, 7.56 mJ cm^{-2} at 0.1 g mL^{-1}, and 32.6 mJ cm^{-2} at 0.5 g mL^{-1}. Insets in (d–f) show the CIE 1931 chromaticity diagram and the coordinates of different PDMS films under different excitation power.

properties of QDs. It is worth mentioning that the CdS band-edge emission intensity of these films exceeds the intensity of Mn^{2+} emission at different excitation power (Figure 3d–f). When the QD concentration of the LPF is 0.001 g mL^{-1}, I_B exceeds I_O at an excitation power of 2.66 mJ cm^{-2}. With the increase of QD concentration, this excitation power also increased. This phenomenon plays an important role in tuning the photoluminescence properties of the LPF. The inset photograph in Figure 3d–f shows the CIE 1931 chromaticity diagram and the coordinates of different LPFs under different excitation powers. All three LPFs exhibit orange color at a low excitation power. When the excitation power increases to 44.7 mJ cm^{-2}, the color of the film with QD concentration of 0.001, 0.1, and 0.5 g mL^{-1}, becomes blue, purple, and white, respectively. The color-changing range shortens with an increase of QD concentration. Additionally, the ratio of I_B/I_O is different at a certain excitation power among the films with different concentration of QDs. A series of LPFs with different colors could be obtained under fixed-excitation-power laser-irradiation, by changing the concentration of the QDs, which would significantly simplify the preparation process.

Fabrication of LPFs grafted CdS/ZnS/ZnS:Mn^{2+}/ZnS QDs and their mechanical and photoluminescence properties as anticounterfeiting materials are shown in **Figure 4**. A bottom-up method is employed to prepare the excitation-power-dependent color-tunable film. As shown in Figure 4b, PDMS containing color tunable QDs is injected into the mold and then dried at 80 °C to form three heart-shaped patterns. The QD concentration of each heart-shaped pattern is 0.001, 0.1, and 0.5 mg mL^{-1}, respectively. The PDMS is coated onto the surface of the mold when the heart-shaped patterns are solidified and then the film forms after drying at 80 °C. Finally, the heart-shaped patterns are sandwiched and coated with PDMS on the other side of the film. As can be seen in Figure 4a, the heart-shaped pattern is almost transparent without irradiation with a laser. The patterns with high concentration (0.5 mg mL^{-1}, right) and middle concentration (0.1 mg mL^{-1}, up) of QDs show yellow color under low-excitation-power laser-irradiation on the surface of the film directly. At the same time, the lowest concentration (0.001 mg mL^{-1}) pattern (left) show amaranth color, and this phenomenon corresponds to the result shown in Figure 3. Next, the excitation power rises to 10 mJ cm^{-2}. The pattern with a high concentration of QDs still keeps the orange color. The color of patterns with middle and low concentration of QDs become white and pink, respectively. When the excitation power continuously rises to 30 mJ cm^{-2}, the color of the patterns with high, middle, and low concentration of QDs show pink, light blue, and blue, respectively. These results confirm that the color change range of LPFs is modulated by the concentration of QDs. Photographs of the as-fabricated LPFs under different excitation power are shown in the bottom of Figure 4a. The difference of color change range among the three patterns can be cleanly observed in this series photographs. The flexibility and stretchable properties of the LPFs are shown in Figure 4c,d. The LPFs can be twisted 180° and stretched more than 50%, and the as-designed luminescent patterns in LPFs

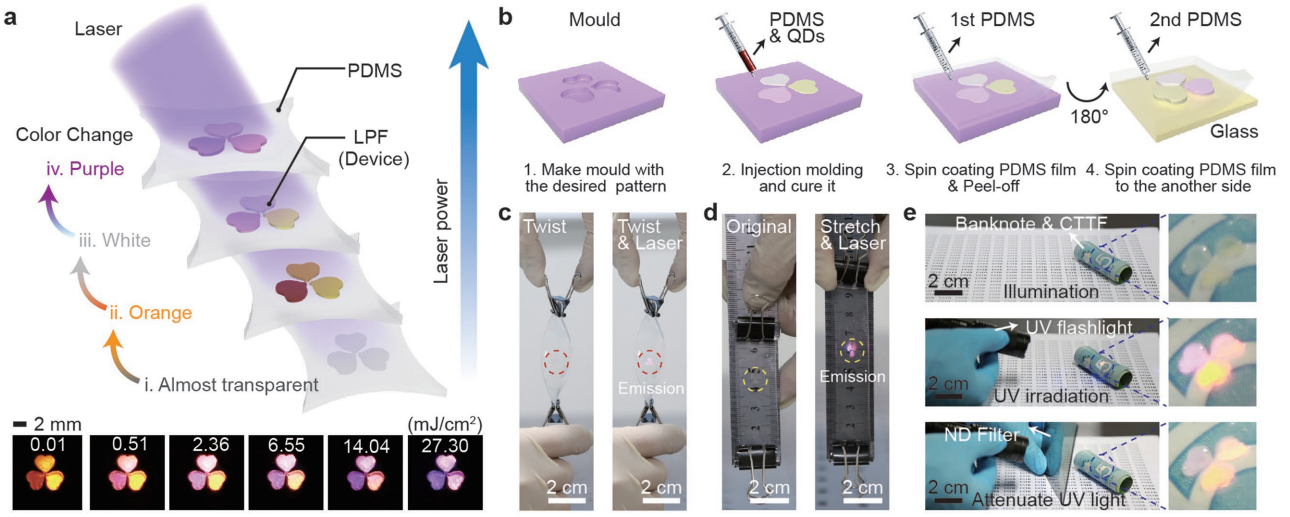

Figure 4. Fabrication of luminescent PDMS film grafted CdS/ZnS/ZnS:Mn^{2+}/ZnS QDs and the mechanical and photoluminescence properties as anticounterfeiting materials. a) Schematic illustration and photographs of luminescent PDMS film irradiated by a laser with different powers. b) The fabrication process of LPF. Photographs showing the c) twisting and d) stretchable properties of LPF. e) Photographs of LPF material in daylight and under a UV flashlight (365 nm). The LPF material is almost transparent in daylight. The power of UV light was attenuated by an ND filter and the as-observed color of LPF is changed depending on the different excitation intensities, to provide the anticounterfeiting effect.

have a corresponding deformation indicating the good compatibility of as-synthesized QDs in PDMS. Figure 4e shows a photograph of the LPFs pasted on a polymer banknote and irradiated with daylight or a commercial UV flashlight. The patterns on the banknote, pasted by the LPFs, can be identified due to the transparency of the film (Figure 4ei). When the LPFs is irradiated by a low-powered UV flashlight, and not the laser light source used in the above photoluminescence measurement, the patterns in the film with different concentrations of QDs also clearly show three colors. Then, a neutral density filter (ND filter) is applied to reduce the irradiation power. As can be seen in Figure 4eiii, the color of the pattern irradiated by lower energy has a slight change compared to that of a pattern irradiated by higher energy, shown in Figure 4eii. This result indicates that the excitation-power-dependent, color-tunable film can be used as an anticounterfeiting material easily, which only needs slight modification of the detector.

3. Conclusion

In summary, we firstly fabricate stretchable PDMS film grafted CdS/ZnS/ZnS:Mn^{2+}/ZnS core/multishell QDs with a unique excitation-power-dependent luminescence property; the LPF shows blue and orange emission simultaneously, and tuning of photoluminescence originates from the variation in the emission intensity ratios. Additionally, the concentration of QDs in the substrates (hexane or PDMS) can also control the photoluminescence tuning. Their mechanisms have been demonstrated and verified experimentally. It is believed that the tunable photoluminescence property of these flexible LPF grafted doped core/shell QDs, which depends on outer excitation power and intrinsic QD concentration, is important for solution-based, color-tunable luminescence materials and devices, and demonstrates an example for anticounterfeiting applications.

4. Experimental Section

Precursor Preparation:

(a) Mn-precursor solution: OLA (4 mL) and $Mn(Ac)_2{\cdot}4H_2O$ (4.9 mg, 0.02 mmol) were added into a 25 mL flask and heated at 80 °C for 10 min under N_2 flow. After a clear solution was obtained, the solution was cooled to room temperature and ready for use. Note that the Mn precursor solution should be freshly made before the synthesis.

(b) Sulfur solution: Sulfur powder (12.8 mg, 0.4 mmol) was added into a flask with ODE (10 mL). Then the solution was heated to 80 °C under N_2 flow. The temperature was maintained for 10 min. After a clear solution was obtained, the solution was cooled to room temperature and ready for use.

(c) Zinc stearate solution: Zinc stearate (0.4 mmol) was added into a flask with ODE (10 mL). After degassing for 10 min, the mixture was heated to 120 °C to dissolve zinc stearate. The solution was cooled to room temperature and slurry formed. The slurry was directly used for ZnS-shell growth.

Synthesis of the Cd Precursor of Cadmium Myristate: In a typical synthesis, a solution of cadmium nitrate in methanol (0.05 m, 40 mL) was added to a solution of sodium myristate in methanol (0.025 m, 240 mL). The resulting white precipitate was washed twice with methanol and dried under vacuum overnight to remove all solvents.

Preparation of CdS: Cadmium myristate (0.1928 g) and S powder (0.0056 g) were loaded into a three-necked flask and mixed with 1-ODE (20 mL). After purging with N_2, the temperature was raised to 240 °C. The reaction was carried out for 20 min and then was allowed to cool to room temperature. The nanocrystals of CdS were precipitated by adding acetone and washed by chloroform and acetone three times. Finally, the CdS nanocrystals were stored in 8 mL hexane.

Overcoating the ZnS shell on the CdS: The hexane solution of CdS core (4 mL) was dissolved in a mixture solution of ODE and oleylamine (12 mL of ODE and 4 mL of oleylamine). After purging with N_2, the solution was heated to 220 °C. The zinc-stearate stock solution (4.8 mL, 0.04 M in ODE) and S stock solution (4.8 mL, 0.04 M in ODE) were introduced to the CdS solution by dropwise addition separately. After 10 min of reaction, another batch of stock solution was added into the CdS solution. The reaction was stopped after 10 min reaction and then

cooled to room temperature. The nanocrystals were precipitated by adding acetone and washed by chloroform and acetone three times and stored in 4 mL hexane.

Mn^{2+}-Dopant Shell and the Outmost ZnS Shell Growth: The hexane solution of CdS/ZnS (4 mL) was added into a mixture solution of ODE and oleylamine (12 mL of ODE and 4 mL of oleylamine), and then hexane was removed by purging of N_2. Then the CdS/ZnS solution was heated to 280 °C. The $Mn(Ac)_2$ stock solution (2 mL, 0.005 M in oleylamine) and S stock solution (0.25 mL, 0.04 M in ODE) were alternatively introduced into the hot solution by dropwise addition. After a further 20 min reaction, the zinc-stearate stock solution and S stock solution were introduced to the CdS/ZnS solution similar to the overcoating of ZnS shell above. Then, a large excess of zinc-stearate stock solution (6 mL) was added into the solution and reacted for 20 min. Finally, 4 mL oleic acid was introduced into the solution and cooled to room temperature. The nanocrystals were precipitated by adding acetone. The nanocrystals were stored in hexane.

Fabrication of Color-Tunable PDMS Film: The PDMS containing the color tunable QDs was injected into the matrix and then dried at 80 °C to form the three heart-shaped patterns. The concentration of QDs of each heart-shaped pattern was 0.001, 0.1, and 0.5 mg mL^{-1}, respectively. The PDMS was coated onto the surface of the matrix when the heart-shaped patterns were solidified. The film can be obtained after drying at 80 °C. Finally, the heart-shaped patterns were sandwiched and coated PDMS on the other side of the film.

Characterization: TEM was performed on a JEM-2010 operated at 120 keV on 200 mesh carbon coated nickel grids. X-ray powder diffraction was performed on a PANalytical X'Pert^3 Powder diffractometer equipped with a Cu Kα radiation source and operated at 40 kV and 40 mA. UV–vis–NIR absorption spectra of colloidal solutions were collected at room temperature using a Varian Cary 5 spectrophotometer. The steady PL spectra were carried out using a FLSP9200 fluorescence spectrophotometer (Edinburgh Instruments Ltd, UK). Excitation dependent photoluminescence signals were collected by an optical fiber and detected using a spectrometer (SD2000, Ocean Optics) with an integration time of 1 s. The samples were excited with the output of a Nd:YAG laser (355 nm, pulse width of about 3–6 ns, repetition frequency of 10 Hz).

Supporting Information

Supporting Information is available from the Wiley Online Library or from the author.

Acknowledgements

F.L. and X.W. contributed equally to this work. The authors thank the support from National Natural Science Foundation of China (Nos. 91622125, 51572023, 61405040, 51622205, 61675027), Natural Science Foundations of Beijing (2172036), Fundamental Research Funds for the Central Universities (FRF-TP-16-002A3), National Key R & D project from Minister of Science and Technology, China (2016YFA0202703), National Postdoctoral Program for Innovative Talents (BX201600040) and China Postdoctoral Science Foundation Funded Project (2016M600976).

Received: January 4, 2017
Revised: February 6, 2017
Published online: March 20, 2017

[1] I. Coropceanu, M. G. Bawendi, *Nano Lett.* **2014**, *14*, 4097.
[2] Y. Shirasaki, G. J. Supran, M. G. Bawendi, V. Bulović, *Nat. Photonics* **2013**, *7*, 13.
[3] L. Etgar, W. Zhang, S. Gabriel, S. G. Hickey, M. K. Nazeeruddin, A. Eychmüller, B. Liu, M. Grätzel, *Adv. Mater.* **2012**, *24*, 2202.
[4] a) F. Zhang, H. Zhong, C. Chen, X.-g. Wu, X. Hu, H. Huang, J. Han, B. Zou, Y. Dong, *ACS Nano* **2015**, *9*, 4533; b) H. Tetsuka, R. Asahi, A. Nagoya, K. Okamoto, I. Tajima, R. Ohta, A. Okamoto, *Adv. Mater.* **2012**, *24*, 5333.
[5] a) B. S. Mashford, M. Stevenson, Z. Popovic, C. Hamilton, Z. Zhou, C. Breen, J. Steckel, V. Bulovic, M. Bawendi, S. Coe-Sullivan, *Nat. Photonics* **2013**, *7*, 407; b) F. Di Stasio, J. Q. Grim, V. Lesnyak, P. Rastogi, L. Manna, I. Moreels, R. Krahne, *Small* **2015**, *11*, 1328.
[6] a) J. Lim, M. Park, W. K. Bae, D. Lee, S. Lee, C. Lee, K. Char, *ACS Nano* **2013**, *7*, 9019; b) X. Yang, D. Zhao, K. S. Leck, S. T. Tan, Y. X. Tang, J. Zhao, H. V. Demir, X. W. Sun, *Adv. Mater.* **2012**, *24*, 4180.
[7] C. Zhao, Z. Bai, X. Liu, Y. Zhang, B. Zou, H. Zhong, *ACS Appl. Mater. Interfaces* **2015**, *7*, 17623.
[8] a) W. Deng, X. Xu, X. Zhang, Y. Zhang, X. Jin, L. Wang, S. T. Lee, J. Jie, *Adv. Funct. Mater.* **2016**, *26*, 4797; b) J. Pan, L. N. Quan, Y. Zhao, W. Peng, B. Murali, S. P. Sarmah, M. Yuan, L. Sinatra, N. M. Alyami, J. Liu, *Adv. Mater.* **2016**, *28*, 8718; c) Z. Ning, X. Gong, R. Comin, G. Walters, F. Fan, O. Voznyy, E. Yassitepe, A. Buin, S. Hoogland, E. H. Sargent, *Nature* **2015**, *523*, 324.
[9] A. P. Alivisatos, *Science* **1996**, *271*, 933.
[10] K. D. Wegner, Z. Jin, S. Lindén, T. L. Jennings, N. Hildebrandt, *ACS Nano* **2013**, *7*, 7411.
[11] W. X. Guo, C. Xu, G. Zhu, C. F. Pan, C. J. Lin, Z. L. Wang, *Nano Energy* **2012**, *1*, 176.
[12] E. Sotelo-Gonzalez, L. Roces, S. Garcia-Granda, M. T. Fernandez-Arguelles, J. M. Costa-Fernandez, A. Sanz-Medel, *Nanoscale* **2013**, *5*, 9156.
[13] Y. Yang, O. Chen, A. Angerhofer, Y. C. Cao, *J. Am. Chem. Soc.* **2006**, *128*, 12428.
[14] a) J. Andres, R. D. Hersch, J. E. Moser, A. S. Chauvin, *Adv. Funct. Mater.* **2014**, *24*, 5029; b) Y. Liu, K. Ai, L. Lu, *Nanoscale* **2011**, *3*, 4804.
[15] a) X. Liu, J. Wang, L. Tang, L. Xie, Y. Ying, *Adv. Funct. Mater.* **2016**, *26*, 5515; b) D.-H. Park, J. Hong, I. S. Park, C. W. Lee, J.-M. Kim, *Adv. Funct. Mater.* **2014**, *24*, 5186; c) L. Gonzalez-García, J. Parra-Barranco, J. R. Sanchez-Valencia, J. Ferrer, M.-C. Garcia-Gutierrez, A. Barranco, A. R. Gonzalez-Elipe, *Adv. Funct. Mater.* **2013**, *23*, 1655; d) M. L. Que, W. X. Guo, X. J. Zhang, X. Y. Li, Q. L. Hua, L. Dong, C. F. Pan, *J. Mater. Chem. A* **2014**, *2*, 13661.
[16] S. Walia, C. M. Shah, P. Gutruf, H. Nili, D. R. Chowdhury, W. Withayachumnankul, M. Bhaskaran, S. Sriram, *Appl. Phys. Rev.* **2015**, *2*, 011303.
[17] a) T. Yamada, Y. Hayamizu, Y. Yamamoto, Y. Yomogida, A. Izadi-Najafabadi, D. N. Futaba, K. Hata, *Nat. Nanotechnol.* **2011**, *6*, 296; b) D. H. Kim, J. Xiao, J. Song, Y. Huang, J. A. Rogers, *Adv. Mater.* **2010**, *22*, 2108; c) X. T. Cao, X. Cao, H. J. Guo, T. Li, Y. Jie, N. Wang, Z. L. Wang, *ACS Nano* **2016**, *10*, 8038; d) X. D. Wang, H. L. Zhang, L. Dong, X. Han, W. M. Du, J. Y. Zhai, C. F. Pan, Z. L. Wang, *Adv. Mater.* **2016**, *28*, 2896.
[18] a) H. Stoyanov, M. Kollosche, S. Risse, R. Wache, G. Kofod, *Adv. Mater.* **2013**, *25*, 578; b) S. J. Benight, C. Wang, J. B. H. Tok, Z. Bao, *Prog. Polym. Sci.* **2013**, *38*, 1961; c) M. Ramuz, B. C. Tee, J. B. Tok, Z. Bao, *Adv. Mater.* **2012**, *24*, 3223; d) D. P. J. Cotton, I. M. Graz, S. P. Lacour, *IEEE Sens. J.* **2009**, *9*, 2008; e) G. F. Hu, R. R. Zhou, R. M. Yu, L. Dong, C. F. Pan, Z. L. Wang, *Nano Res.* **2014**, *7*, 1083; f) X. Wang, L. Dong, H. Zhang, R. Yu, C. Pan, Z. L. Wang, *Adv. Sci.* **2015**, *2*, 1500169.
[19] a) A. J. Bandodkar, R. Nunez-Flores, W. Jia, J. Wang, *Adv. Mater.* **2015**, *27*, 3060; b) J. Yoon, S. Y. Hong, Y. Lim, S. J. Lee, G. Zi, J. S. Ha, *Adv. Mater.* **2014**, *26*, 6580; c) M. Shin, J. H. Song,

G. H. Lim, B. Lim, J. J. Park, U. Jeong, *Adv. Mater.* **2014**, *26*, 3706; d) C. Yan, W. Kang, J. Wang, M. Cui, X. Wang, C. Y. Foo, K. J. Chee, P. S. Lee, *ACS Nano* **2013**, *8*, 316; e) D. H. Kim, R. Ghaffari, N. Lu, J. A. Rogers, *Annu. Rev. Biomed. Eng.* **2012**, *14*, 113; f) K. S. Kim, Y. Zhao, H. Jang, S. Y. Lee, J. M. Kim, K. S. Kim, J. H. Ahn, P. Kim, J. Y. Choi, B. H. Hong, *Nature* **2009**, *457*, 706; g) C. F. Pan, M. X. Chen, R. M. Yu, Q. Yang, Y. F. Hu, Y. Zhang, Z. L. Wang, *Adv. Mater.* **2016**, *28*, 1535.

[20] a) K.-S. Sohn, S. Timilsina, S. P. Singh, J.-W. Lee, J. S. Kim, *ACS Appl. Mater. Interfaces* **2016**, *8*, 34777; b) C. Yan, J. Wang, X. Wang, W. Kang, M. Cui, C. Y. Foo, P. S. Lee, *Adv. Mater.* **2014**, *26*, 943; c) S. H. Chae, W. J. Yu, J. J. Bae, D. L. Duong, D. Perello, H. Y. Jeong, Q. H. Ta, T. H. Ly, Q. A. Vu, M. Yun, X. Duan, Y. H. Lee, *Nat. Mater.* **2013**, *12*, 403; d) S. Cheng, Z. Wu, *Adv. Funct. Mater.* **2011**, *21*, 2282; e) C. Yu, Z. Wang, H. Yu, H. Jiang, *Appl. Phys. Lett.* **2009**, *95*, 141912; f) R. Bao, C. Wang, L. Dong, R. Yu, K. Zhao, Z. L. Wang, C. Pan, *Adv. Funct. Mater.* **2015**, *25*, 2884; g) R. R. Bao, C. F. Wang, L. Dong, R. M. Yu, K. Zhao, Z. L. Wang, C. F. Pan, *Adv. Funct. Mater.* **2015**, *25*, 2884; h) X. Wang, H. Zhang, R. Yu, L. Dong, D. Peng, A. Zhang, Y. Zhang, H. Liu, C. Pan, Z. L. Wang, *Adv. Mater.* **2015**, *27*, 2324; i) R. R. Zhou, G. F. Hu, R. M. Yu, C. F. Pan, Z. L. Wang, *Nano Energy* **2015**, *12*, 588.

[21] a) J. S. Steckel, J. P. Zimmer, S. Coe-Sullivan, N. E. Stott, V. Bulovic, M. G. Bawendi, *Angew. Chem., Int. Ed. Engl.* **2004**, *43*, 2154; b) Y. Shirasaki, G. J. Supran, M. G. Bawendi, V. Bulović, *Nat. Photonics* **2012**, *7*, 13.

[22] a) M. Geszke-Moritz, H. Piotrowska, M. Murias, L. Balan, M. Moritz, J. Lulek, R. Schneider, *J. Mater. Chem. B* **2013**, *1*, 698; b) B. B. Srivastava, S. Jana, N. S. Karan, S. Paria, N. R. Jana, D. D. Sarma, N. Pradhan, *J. Phys. Chem. Lett.* **2010**, *1*, 1454.

[23] L. Brus, *J. Chem. Phys.* **1983**, *79*, 5566.

[24] S. Fery-Forgues, D. Lavabre, *J. Chem. Educ.* **1999**, *76*, 1260.

[25] O. Chen, D. E. Shelby, Y. Yang, J. Zhuang, T. Wang, C. Niu, N. Omenetto, Y. C. Cao, *Angew. Chem., Int. Ed. Engl.* **2010**, *49*, 10132.

[26] W. R. Algar, D. Wegner, A. L. Huston, J. B. Blanco-Canosa, M. H. Stewart, A. Armstrong, P. E. Dawson, N. Hildebrandt, I. L. Medintz, *J. Am. Chem. Soc.* **2012**, *134*, 1876.